Applied Clay Science 137 (2017) 233–240

Contents lists available at ScienceDirect

Applied Clay Science

journal homepage: www.elsevier.com/locate/clay

Research paper

Extended and local structural characterization of a natural and 800 °C fired Na-montmorillonite–Patagonian bentonite by XRD and Al/Si XANES

L. Andrini [a], R. Moreira Toja [b,c], M.R. Gauna [b], M.S. Conconi [b], F.G. Requejo [a], N.M. Rendtorff [b,c,*]

[a] Instituto de Fisicoquímica Teórica y Aplicada (INIFTA): (UNLP-CONICET La Plata), 64 y Diagonal 113, 1900 La Plata, Argentina
[b] Centro de Tecnología de Recursos Minerales y Cerámica (CETMIC): (CIC-CONICET-CCT La Plata), Camino Centenario y 506, C.C.49 (B1897ZCA), M.B. Gonnet, Argentina
[c] Dpto. de Química, Facultad de Ciencias Exactas, Universidad Nacional de La Plata, UNLP, 47 y 115, 1900 La Plata, Argentina

ARTICLE INFO

Article history:
Received 1 November 2016
Received in revised form 16 December 2016
Accepted 18 December 2016
Available online 29 December 2016

Keywords:
Bentonite
Montmorillonite
Fired bentonite
Structure
XANES

ABSTRACT

A structural characterization of a Patagonian bentonite and its corresponding heating product (800 °C) was carried out. The nature of aluminum and silicon atoms was investigated using Al and Si K-XANES spectroscopy and compared with other well-known Al and/or Si containing materials.
The studied material comes from Lago Pellegrini area-Rio Negro Province, Argentina. The main crystalline phase was confirmed to be a Na-montmorillonite. The thermal behavior was studied by DTA-TG-DTG and XRD. A Rietveld based quantification was performed as complementary study. About 90% Na-montmorillonite (clay mineral of smectite Group) content was confirmed and different impurities (quartz, gypsum and feldspars) were also quantified. The smectitic interlayer thermal displacement was determined between 15.49 and 9.81 Å. The XANES results allowed obtaining the Al^{IV}/Al^{VI} ratio and the local symmetry and distortions at Si and Al-sites.
The tetra-coordination of silicon and the aluminum tetra and hexa-coordinated was found in both materials. The expected high Al^{IV}/Al^{VI} ratio was confirmed and pondered for the thermally treated bentonite.

1. Introduction

Clay minerals are widely used in various industrial applications owing to their physicochemical properties such as high surface area and porosity, low specific gravity, adsorption and ionic exchange capacities, crystal morphology, composition hydration and swelling abilities, as well as their catalytic and other properties. These minerals are widely used in many industrial processes such as effective sources of protons in paper and ceramic industry; as suspending medium in saltwater drilling fluids, paints, and pharmaceuticals; as absorbents in pet litter, agricultural chemicals, water, and oil sorption industries; as well as in the cosmetic sector, among many more (Murray, 2000; Grim and Güven, 1978). The application of these materials in polymer industry is also very important (Liu, 2007). Most of these features of clay minerals can be improved and changed by making use of acid activation, soda activation, ion exchange, and thermal treatment processes (Barrer, 1989; Besq et al., 2003; Christidis, 1998; Grim and Güven, 1978; Komadel, 2016; Mahmoud, 1999; Reichle, 1985; Reis and Ardisson, 2003; Sarikaya et al., 2000; Tan et al., 2004).

Bentonite is a colloidal, alumino-silicate rock derived from weathered volcanic ash, which is composed by more than 70% smectite. Accessory minerals quartz, opal, mica, feldspar, gypsum, calcite and zeolites are frequents (Grim and Güven, 1978). Smectite group minerals (2:1 layer phyllosilicate clay minerals) have a structure composed by one sheet of octahedral (O) Al placed between two sheets of tetrahedral (T) Si, with substitutions of some tetrahedral Si atoms by Al atoms and/or of octahedral atoms (Al^{3+} or Mg^{2+}) substituted by atoms with lower oxidation number (Grim and Güven, 1978). The net negative charge of the 2:1 (TOT) layers is balanced by the exchangeable cations such as Na^{+} and Ca^{2+} located between the layers and around the edges (Komadel, 2016; Önal and Sarıkaya, 2007). Basal spacing, d(001), for air dried smectites, changes from 12.6 to 15.4 Å depending on type and valence of the exchangeable cations.

Bentonite rocks may be subjected to high temperatures in some applications including foundry, porous ceramic materials (Gunay and Ozkan, 2001), catalysts (Pinnavaia, 1983; Reichle, 1985), treatment of aqueous solution (Divakar et al., 2008), civil engineering, and others (Abu-Zreig et al., 2001). Some physico-chemical properties of smectites such as swelling, plasticity, cohesion, compressibility, strength, cation-exchange capacity, particle size, adsorptive properties, pore structure, surface area, acidic character, and catalytic activity as well as mineralogy are greatly affected by thermal treatment (Grim and Güven, 1978; Önal and Sarıkaya, 2007; Wang et al., 1990; Gunay and Ozkan, 2001).

* Corresponding author at: Centro de Tecnología de Recursos Minerales y Cerámica (CETMIC): (CIC-CONICET-CCT La Plata), Camino Centenario y 506, C.C.49 (B1897ZCA), M.B. Gonnet, Argentina.
E-mail address: rendtorff@cetmic.unlp.edu.ar (N.M. Rendtorff).

http://dx.doi.org/10.1016/j.clay.2016.12.030
0169-1317/

Thus, the thermal treatment changes in the physical, chemical and mechanical properties of these clays depend on their mineralogy and crystal structures. Therefore, the utilization of these minerals as raw materials in possible applications requires knowledge of the detailed response of their variations with temperature. This fact determines the requirement of multiple characterization techniques to fundamentally understand both the native system and its thermal evolution, and consequent changes in the physicochemical properties.

X-ray Absorption Spectroscopy (XAS) is a powerful technique for obtaining electronic and structural information. It consists in an element-specific method capable of providing quantitative information on the local coordination environment around absorbing atoms in crystalline or amorphous systems (Fendorf et al., 1994). The XANES (X-ray Absorption Near Edge Structure) region of the spectrum is sensitive to the valence state of the central atom and the geometry and types of surrounding atoms (Henderson et al., 2014). XANES, unlike XRD though complementary, is a technique of local-scale order.

These sets of techniques have optimum potential for the characterization of complex systems such as bentonite and its heated product prepared by thermal processing of the same bentonite. We propose, in this paper, to study the structural conformations in commercial industrial grade material (rock) as local and long-range changes induced by thermal effects. Particularly in this work, assess the structure of a fired Na dioctahedral montmorillonite present in a Patagonian bentonite and the resultant material treated at 800 °C (meta-montmorillonite) in air using Differential Thermal Analysis (DTA), Thermogravimetric Analysis (TG), conventional X-ray powder diffraction (XRD) and aluminum-silicon near edge K XANES.

2. Materials and methods

A commercial sodium Patagonian bentonite that comes from Lago Pellegrini area -provincia de Río Negro, Argentina, was studied (Del Lago bentonite (Castiglioni Pes y Cia.). Its mineralogy was described as a dioctaedric smectite montmorillonite type (>94–99%) with traces of quartz, lithoclasts, glass shards, zeolites, feldspar, micas, gypsum, and sometimes calcite (Vallés and Impiccini, 1999).

It must be considered that the bentonite quality varies according with the exploited working front. There are other bentonite localities in Patagonia. The structural characterization refers exclusively to Na-montmorillonite that is the major mineral phase at the Lago Pellegrini bentonite.

Particularly the studied material presents a specific weight of 2.21 g/cm^3 and an apparent specific weight of 0.95 g/cm^3. It is commercialized in standard mesh #200. A 6 wt.% water suspension presents an 8.5 pH; the Mohs hardness is between 1 and 1.5. The de-agglomerated powder mean particle size is below the micron. The chemical composition of a dried sample (evaluated by Inductively Coupled Plasma Atomic Emission Spectroscopy - ICP-EAS) together with the mass loss after heating at 1000 °C are shown in Table 1.

Table 1
Dried 110 °C bentonite chemical analysis.

Oxide	wt.%
SiO_2	57.27
Al_2O_3	21.24
Fe_2O_3	4.45
Na_2O	2.76
MgO	2.71
SO_3	2.40
CaO	1.10
TiO_2	0.38
K_2O	0.26
Lost on ignition (1000 °C)	7.31

A fired Bentonite was also characterized, setting the heating program in order to ensure complete dehydration and dehydroxilation. The sample was fired in an electric furnace in air atmosphere up to 800 °C with 10 °C/min as heating rate and with 15 min of dwell. A porcelain crucible was employed for treating 20 g. Making an analogy with kaolinitic clays, the phase obtained by firing the montmorillonite clay mineral can be designated as meta-montmorillonite (Zivica and Palou, 2015). The original and fired samples were labeled Bent-0 and Bent-800 respectively.

As reference samples for absorption XANES technique, the following standards were used: (a) for Si K-edge XANES: synthetic amorphous silicon dioxide (Am-SiO_2), commercial float glass, commercial kaolinitic clay (98%, Fischer, Georgia, USA), commercial pyrophyllite (95%) and kyanite (95%); (b) for Al K-edge XANES: synthetic α-Al_2O_3 (ALCOA 99.5%), commercial gibbsite (ALCOA 99.5%), and mullite (95%, Synthetic Mullite M72, VAW, Veremigte, Werke AG, Germany).

Identification and quantification of crystalline phases in the clays and fired materials were carried out by X-ray diffraction (XRD) (Philips 3020 with Cu-Kα radiation, Ni filter, at 40 kV–35 mA); with 0.04° and 2 s steps in the 3–80° range. The employed quantification method was fully described in two previous works (Conconi et al., 2014; Serra et al., 2013). The XRD patterns were analyzed with the program FullProf (Version 5.40, March 2014) which is a multipurpose profile-fitting program (Rodríguez-Carvajal, 2001), including Rietveld refinement to perform phase quantification (Rietveld, 1969).

The effect of heat treatment was also evaluated by thermogravimetric analysis and differential thermal analysis (DTA-TG) simultaneously carried out on a Rigaku Evo2 equipment with 10 °C/min as heating rate in Pt crucibles in air atmosphere. The derivative curve of the TG (DTG) was also employed for this purpose.

XANES experiments were performed in the Soft X-rays Spectroscopy (SXS) beamline of the Brazilian Synchrotron Light Laboratory (LNLS, Campinas, SP, Brazil). The beam focalization was performed using a Ni mirror. For Al K-edge, the monochromator employed was YB66, with a resolution of about 2 eV with a slit aperture of 2 mm. For Si K-edge, the monochromator employed was InSb(111), with a resolution of about 1 eV with a slit aperture of 1 mm. The I_0 incident photon flux intensity was measured using a mesh of Au located before the main chamber. The photon energies were calibrated using an Al (Si) metallic foil and setting the first inflection point to the energy of the K absorption edge of Al^0 at 1559 eV (Si^0 at 1839 eV). The spectra were acquired at room temperature and the pressure chamber was about 10^{-4} Torr. The aluminosilicate minerals were ground into fine powder (standard mesh # 200), and the powder samples were pressed uniformly on electric carbon tape supported on a stainless-steel sample holder for XANES measurements. The angle between the sample holder and the detector was 45°.

All spectra were processed by standard methods from I_f/I_0 signal analysis, where I_f is the detected fluorescence intensity. The pre-edge and the normalization background were realized by *Athena* (Ravel and Newville, 2005). To exclude self-absorption effects were compared the spectra obtained by fluorescence mode with those obtained by Total Eletron Yield (TEY) mode at Si K-edge. After background subtraction and normalization, the characteristic resonance peaks in the XANES region was fitted using Gaussian functions and the continuum step was fitted using arctan functions (Outka and Stöhr, 1988) using WinXAS3.1 (Ressler, 1998).

3. Results and discussion

3.1. Mineralogical analysis of the studied industrial Na-montmorillonite–Patagonian bentonite and the heated (800 °C) material by XRD

Fig. 1 shows the XRD patterns of both materials studied, Bent-0 and Bent-800 in the 3–80° 2θ range; principal reflections are labeled. The corresponding identified crystalline phases are shown in Table 2,

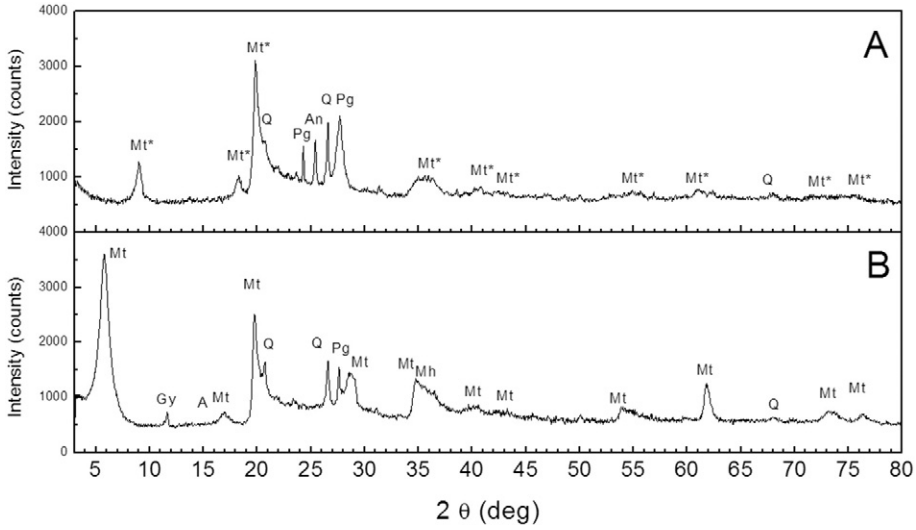

Fig. 1. XRD patterns of the studied metabentonite (A) and bentonite (B). (Mt: Montmorillonite; Mt*: Dehydrated Montmorillonite, Q: Quartz, Gy: Gypsum, Pg: Plagioclase, An: Anhydrite, and A: Analcime).

together with the ideal formula and the scored PDF card from the International Centre for Diffraction Data. For the as received bentonite (Bent-0), the principal crystalline phase corresponds to a Smectite, more specifically to Na-montmorillonite. As expected for this kind of mineral (Grim and Güven, 1978), it is accompanied by quartz, gypsum and feldspars (in this case, plagioclase). The results of the Rietveld based quantification are shown in Table 3. The amount of montmorillonite (Mt) quantified was in accordance with expected values. The Rwp parameter resulting values were in all cases below 30, sustaining the goodness of the refinements for this kind of materials.

The detected crystalline phases were in concordance with similar studies (Volzone and Sanchez, 1993; Vallés and Impiccini, 1999). The Gypsum dehydration into anhydrite occurs at intermediate temperatures (150–300 °C), hence, anhydrite will be expected in the heated bentonite.

The 001 smectitic reflection was analyzed. This evolved from 5.7° to 9.0° in samples Bent-0 and Bent-800. This can be explained by a decrease in the distance between the interlayers of the clay mineral, due to the water losses observed by the performed thermal analysis. The interlayer distances, estimated from Bragg law, are 15.49 Å and 9.81 Å for montmorillonite in Bent-0 and the dehydrated montmorillonite in Bent-800, respectively. These values are in concordance with reported values (Sarikaya et al., 2000; Sarı Yılmaz et al., 2013). The intensity and shape of the dehydrated montmorillonite (Mt*) principal reflection in the Bent-800 diffraction pattern sustains the fact that the meta montmorillonite structure remains with high enough crystalline grade. This crystalline (lower) structure can be described by the local characterizations of the X-ray spectroscopy showed in the next section.

3.2. Thermal behavior analyses: DTA-TG-DTG.

These analyses revealed that the dehydration and the dehydroxylation stages proceed in two regions: 38–150 °C and 150–720 °C at 10 °C/min of heating rate (see Fig. 2). The corresponding mass losses were 15.46% and 3.74% (total mass loss 17.70%). The mass loss of dehydroxylation reaction is in a good agreement with the previous study (Önal and Sarıkaya, 2007; Wang et al., 1990) and with the evaluated mass loss (Fig. 1). The dehydration of the studied bentonite was complex with three overlapping stages, while its dehydroxylation was observed in a single stage reaction, all of which were represented in the DTG, the local minimums are indicated in the figure. The third step in the dehydratation process could be associated to gypsum dehydratation while the two initial stages correspond to smectite interlamellar water loss.

The 2.40% content of SO_3 (Table 1) implies a higher gypsum content than that found with the Rietveld quantification. This methodology might present significant uncertainties when quantifying minor minerals.

The endothermic dehydration stages can be observed in the DTA curve; temperatures shown in the figure correspond to simultaneous analyses and to the one observed in similar materials (Önal and Sarıkaya, 2007; Wang et al., 1990). The "s" shape signal observed in the DTA between 920 and 1020 °C corresponds to the recrystallization of the bentonite and recrystallization of new phases, respectively, no mass loss would be associated to these processes. Considering this analysis, it can be ensure that a sample heated at 800 °C with the mentioned heating program would be dehydrated and dehydroxilated. These

Table 2
Bent 0 and Bent 800 identified X-ray crystalline phases. Chemical formulas and respective Si–Al atoms coordination taken from the PDF cards-International Center for Diffraction Data.

					Coordination	
Mineral phases	Phase	Ideal formula	Reference	PDF card	Al	Si
Smectite clay group	Montmorillonite	$(Na,Ca)_{0.33}(Al,Mg)_2\ (Si_4O_{10})(OH)_2\cdot 4H_2O$	Mt	00-029-1498	4 and 6	4
	Dehydrated montmorillonite	$(Na,Ca)_{0.33}(Al,Mg)_2\ (Si_4O_{10})(OH)_2$	Mt*		4 and 6	4
Other	Quartz	SiO_2	Qz	00-046-1045		4
mineral phases	Gypsum	$CaSO_4\cdot 2H_2O$	Gy	00-021-0816	–	–
	Feldspars (plagioclase) albite calcian	(Na,Ca) (Si, Al)4O8	Pg	00-020-0548	4	4
	Anhydrite	$CaSO_4\cdot$	An	00-037-1496	–	–
	Analcime	$Na(AlSi_2O_6)\ (H_2O)$	A	00-041-1478	?	?

Table 3
Rietveld quantification of the Bent-0 sample.

Mineral	Weight content (%)
Montmorillonite	90
Feldspars (plagioclase	4
Quartz	3
Gypsum	2
Analcime	1

processes would result in important changes from the structural point of view; the interlayer distance between TOT would decrease because of the loss of both hydroxyl groups and interlayer water. The TOT layers structure of the clay mineral remains in the meta-montmorillonite phase of the heated bentonite. This change was observed by performed XRD analysis (see Fig. 1).

3.3. Si-K XANES analysis

Fig. 3 shows the normalized Si-K XANES spectra of references (quartz, kianite, kaolinite and pyrophyllite), and Fig. 4 shows the XANES spectra corresponding to samples Bent-0, Bent-800 and amorphous silica (Am). For Bent-0 and Bent-800, the obtained spectra are similar to montmorillonite and bentonite spectra reported by Shaw et al. (2009). The absorption edge is at 1845.4 eV, 0.3 eV shifted to higher energy with respect to the corresponding one for amorphous silica.

The main features of the spectra are analyzed by least square fitting, following similar analyses already reported in the literature (L. Andrini et al., 2016a; Li et al., 1994). Fig. 4 shows the fits for the spectra of amorphous silica (Am-SiO_2), Bent-0 and Bent-800. In Table 4 the main characteristics of each resonance for each of the three spectrums (Li et al., 1996, 1994, 1993) are reported. Linear fits (not showed here) between the quartz spectra and Bent-0 spectra cannot reproduce the corresponding Bent-800 spectrum. From a visual inspection between the spectra of quartz and Bent-800, it can be seen that they not share common characteristics. As a second observation it is worth noting the absence of the peak A in both Bent-0 and Bent-800 spectra. The occurrence of this peak is attributed to the presence of distortions in the system or to an increase in the coordination number (Li et al., 1993). The reason of this assignment is because this peak is attributed to the transition of Si 1 s electrons to the antibonding 3s-like state, Si 1s → a_1(Si 3s–3p), forbidden by the dipole selection rules ($\Delta L = \pm 1$, $\Delta S = 0$, $\Delta J = \pm 1$), making the peak A very weak. Thus, it can be concluded that Si occupies tetrahedral sites undistorted in Bent-0, as it expected, and LSO in Bent-800 sample. This result indicates that the thermal treatment does not significantly modify the structure of the Si-local environment.

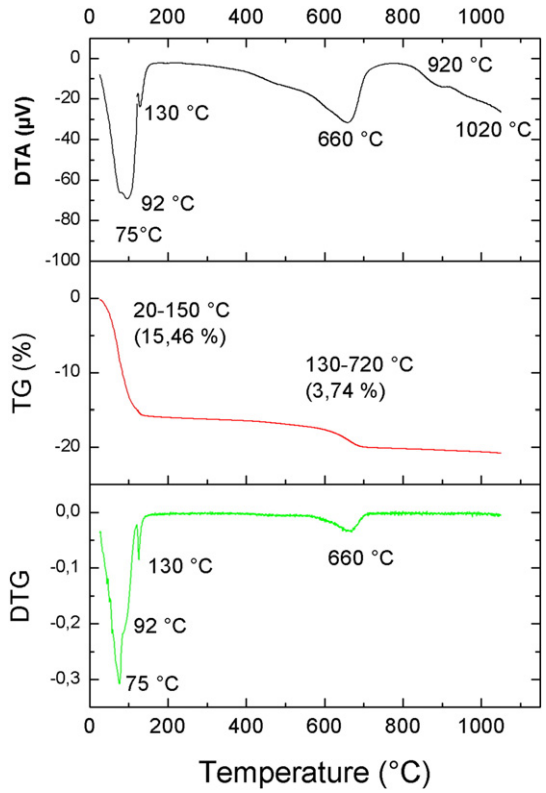

Fig. 2. Bent-0 DTA-TG-DTG analysis.

From the information available in Table 4, it is observed a decrease in all intensities of all resonances in the absorption spectrum for Bent-800 regarding to intensities of the corresponding Bent-0 spectra. The most important diminution is for the Si 1s → t_2 (Si 3p–3s) transition, which provides information of the Si-3p unoccupied, states (Shaw et al., 2009). This can be associated with the processes of dehydroxylation suffered by heated the clay material: losing H atoms, the O atoms have a greater availability of electrons that can fill this t_2-orbital.

3.4. Al-K XANES analysis

Fig. 5 shows the normalized Al-K XANES spectra of reference compounds α-Al_2O_3, gibbsite, kyanite, kaolinite, and mullite. Fig. 6 shows the corresponding spectra and their fittings for Bent-0 and Bent-800 samples. The peak A is associated with the 1s → a_1 (3 s) transition for four coordinate aluminum and the 1s → a_{1g} (3s) transition for hexacoordinated aluminum. Both are forbidden dipolar transitions, and their intensity is then very weak in general. Peak C is associated with the 1s → t_2 (3p) transition for four coordinate aluminum and occurs between 1566.5 and 1567.3 eV, whereas for aluminum hexacoordinated it is associated with the 1s → t_{1u} (3p) transition and it is located between 1568.2 and 1569.1 eV. The peak D is associated with multiple dispersions for both coordinations, and it is more noticeable in four coordinate aluminum centers. The peak E is associated with the 1s → e (3d) transitions for four coordinated aluminum and it is between 1572.7 and 1575.6 eV, whereas for aluminum hexacoordinated, it is associated with the 1s → t_{2g} (3d) transition and it is located between 1572 and 1574.2 V. This information is summarized in Table 5. From these assignments, it is inferable that gibbsite, kyanite and kaolinite have only hexacoordinated aluminum, while the α-alumina has only tetracoordinated aluminum. Finally, mullite contains both tetracoordinated and hexacoordinated aluminum (L. Andrini et al., 2016b).

For the corresponding Bent-0 XANES spectrum it is noted the A peak presence. This peak is usually a small shoulder, because its origin is due to quadrupole transitions. An interpretation of the origin of this transition is associated with the distortion of the tetrahedrons (Romano et al., 2000). This allows interpreting that the Al-tetrahedrons are distorted in the Bent-0. The absence of this peak in Al K XANES for Bent-800 allows us to infer that no distorted Al-tetrahedrons are present.

Following the methodology proposed by Ildefonse et al. (1998)) and Kato et al. (2001) we can assign the peak C to the presence of tetrahedral aluminum and peak D to the presence of octahedral aluminum. Then the areas (see intensity in Table 5), obtained by corresponding fitting to such peaks, are proportional to the number of atoms with these coordinations. We can then calculate the relative proportion of the tetrahedral aluminum. For Bent-0, the calculated Al^{IV}/Al^{total} ratio is 31.13%, and for Bent-800 is 66.45%. To explain this difference, we should note that the experimental spectrum obtained for Bent-800 is like the reported one for montmorillonite and thermally treated montmorillonite (Shaw et al., 2009), and smectites (Ildefonse et al., 1998). Thus, we

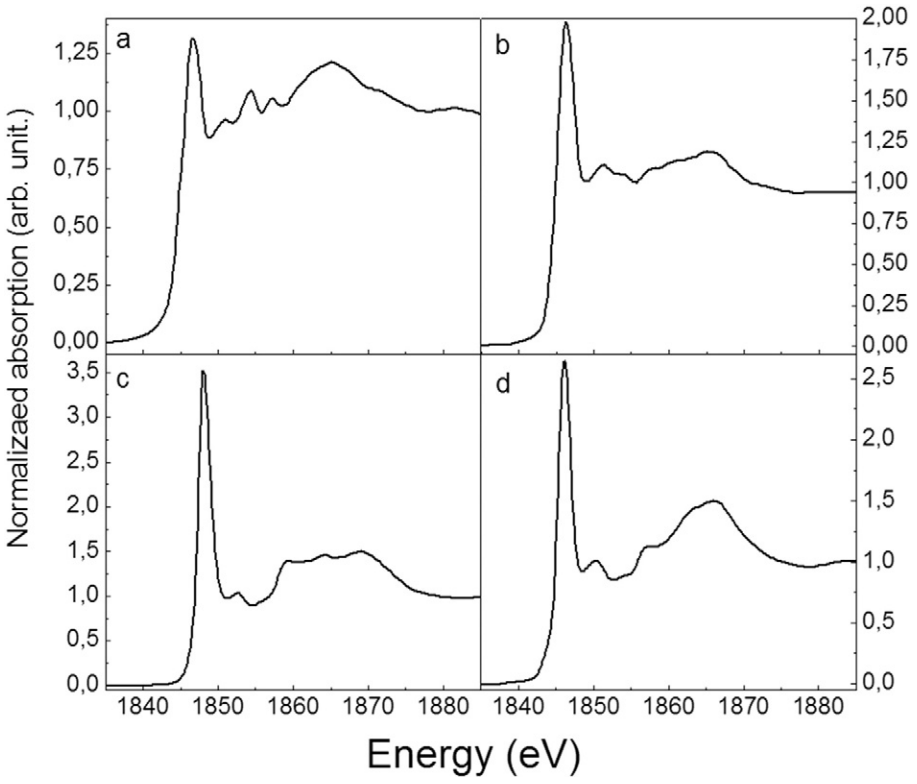

Fig. 3. Si-K XANES spectra of reference compounds: (a) quartz; (b) kianite; (c) kaolinite; and (d) pyrophyllite.

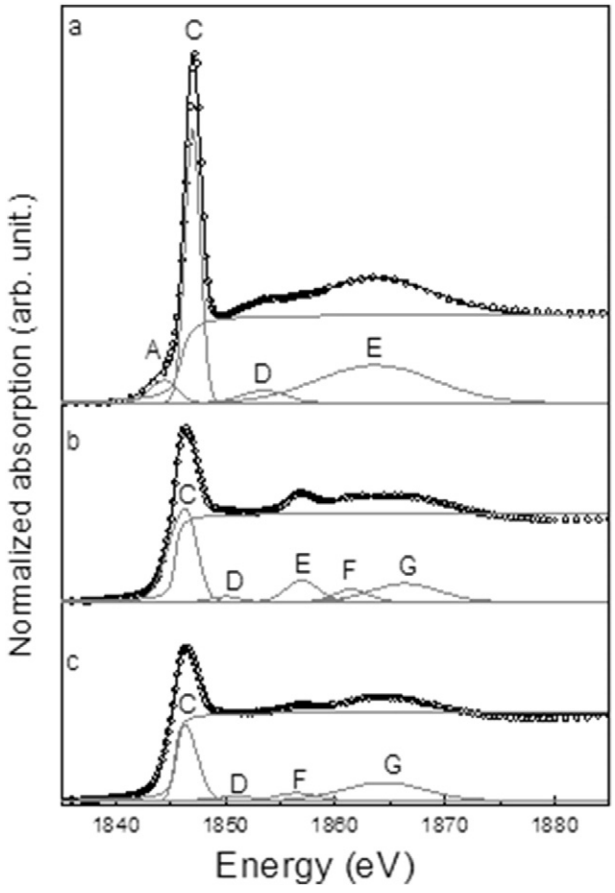

Fig. 4. Si-K XANES spectra of: (a) amorphous SiO_2; (b) Bent-0; and (c) Bent-800. The open circles correspond to the experimental data and full line corresponds to the different fittings.

can assume that the fitting for the peak C in the Al K XANES spectra for Bent-800 contains two peaks overlapped: one related to tetracoordinated aluminum, which in the literature is generally associated with glass phase or a minor order crystallographic arrangement, and another associated with the four-coordinated aluminum in the smectite phase. The way to confirm this assumption is even by simulations, and/or by empirical way, obtaining the XANES spectra of glassy phase and pure smectite one, performing linear overlays to achieve the experimental spectrum.

As it was mentioned in the section of Si-K XANES analysis, the tetrahedron silicon is highly stable to heat treatments. This tetrahedral

Table 4
General characteristics of the Si-K XANES spectra obtained by least square fitting.

Sample	Resonance[a]	Transition[b]	Position (eV)[c]	Intensity (arb. units)
Am-SiO_2	A	Si 1s → a_1(Si 3s–3p)	1844.3	0.78
	C	Si 1s → t_2 (Si 3p–3s)	1847.0	5.47
	D	Multiple scattering	1853.5	08
	E	Si 1s → e (Si 3d–3p)	1863.6	5.7
	F	Multiple scattering	x	x
	G	Si 1s → t_2 (Si 3d–3p)	x	x
Bent-0	A	Si 1s → a_1(Si 3s–3p)	x	x
	C	Si 1s → t_2 (Si 3p–3s)	1846.4	3.40
	D	Multiple scattering	1850.0	0.19
	E	Si 1s → e (Si 3d–3p)	1857.0	0.89
	F	Multiple scattering	1861.4	0.54
	G	Si 1s → t_2 (Si 3d–3p)	1866.3	1.60
Bent-800	A	Si 1s → a_1(Si 3s–3p)	x	x
	C	Si 1s → t_2 (Si 3p–3s)	1846.4	2.98
	D	Multiple scattering	1850.1	0.04
	E	Si 1s → e (Si 3d–3p)	x	x
	F	Multiple scattering	1856.8	0.31
	G	Si 1s → t_2 (Si 3d–3p)	1864.2	1.56

[a] Notation used by (Garvie and Buseck, 1999).
[b] Nomenclature used by (Li et al., 1994).
[c] With an error of 0.3 eV.

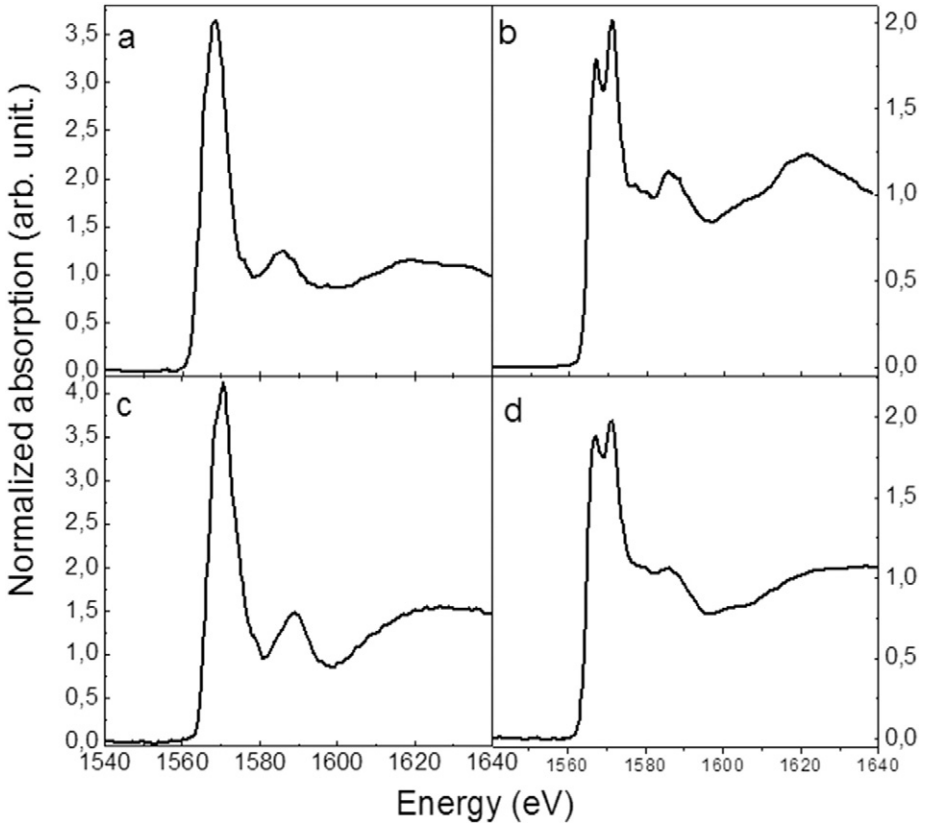

Fig. 5. Al-K XANES spectra of standards: (a) gibbsite; (b) kianite; (c) kaolinite; and (d) mullite. For the nomenclature of the peaks we follow the convention used by (Li et al., 1995). The first Gaussian (A) is located at 1566.8 eV with low intensity. The second Gaussian (C) is located 1567.7 eV with the highest intensity. The third Gaussian (D) and fourth Gaussian (E) are located at 1570.5 and 1573.1 eV respectively.

silicon is maintained in all phases of the samples, which is consistent with the stability of the position and shape of peak C. Additionally, the variation of the ratio between four-coordinated aluminum atoms and the total aluminum atoms could be explained by the appearance of crystalline and amorphous phases. The lack of detection of these new phases in the diffraction patterns, *i.e.* the presence of new phases with tetracoordinated aluminum, could be explained by the appearance of local arrangements, with dimensions of only few nanometers that do not contribute to diffraction. This proposal is consistent with the results previously obtained (Drits et al., 1995). In those experiments, the authors argue that, after heating montmorillonite, the octahedral aluminum atoms become not regular five-fold prism, as the oxygen atoms surrounding the aluminum are in a geometry that is not pyramidal (square base) or bipyramidal (triangular base). This is consistent with the lower reflection height of dehydrated smectite phase in the

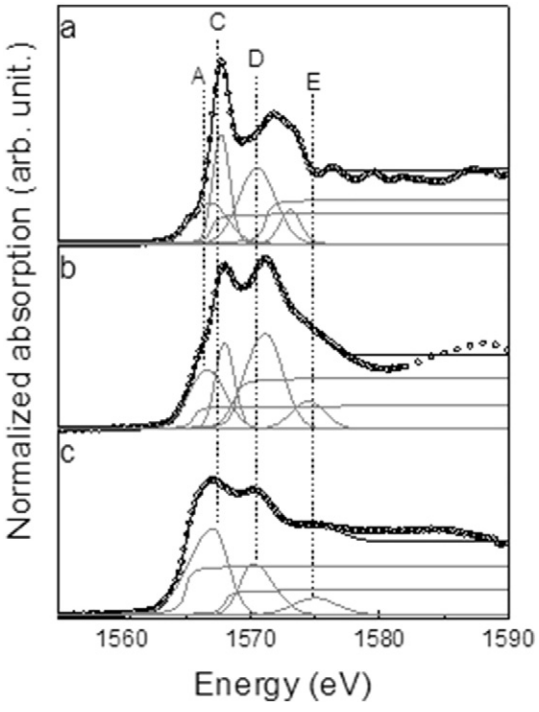

Fig. 6. Al-K XANES spectra of: (a) α-Al_2O_3; (b) Bent-0; and (c) Bent-800. The open circles correspond to the experimental data and full line to fitted results.

Table 5
General characteristics of the Al K XANES spectra obtained by least square fitting.[a]

Sample	Resonance	Transition*	Position (eV)[a]	Intensity (aa. uu.)
Al_2O_3	A	Al 1s → a_1 (Al 3s)	1566.8	1.92
	C	Al 1s → t_2 (Al 3p)	1567.7	2.43
	D	Multiple scattering	1570.5	3.61
	E	Al 1s → t_e (Al 3d)	1573.1	0.93
Bent-0	A	Al 1s → a_{1g} (Al 3s)	1566.6	2.82
	C	Al 1s → t_{1u} (Al 3p)	1567.9	2.13
	D	Multiple scattering	1571.1	4.72
	E	1s → t_{2g} (Al 3d)	1574.4	1.24
Bent-800	A	X	x	x
	C	Al 1s → t_{1u} (Al 3p)	1567.1	4.47
	D	Multiple scattering	1570.1	2.26
	E	1s → t_{2g} (Al 3d)	1575.0	0.96

Notation and nomenclature used by (Li et al., 1995).
[a] With an error of 0.2 eV.

diffraction pattern of Bent-800 sample compared to the reflection of the smectite phase observed in the diffraction patterns for Bent-0.

4. Conclusions

The layered structure of studied clay was deeply solved by the combination of three techniques. Natural (industrial grade) Na-montmorillonite–Patagonian bentonite and its corresponding heated product (obtained after a simple 800 °C treatment) were studied. The extended and local range order structure characterization was carried out by means of two X-ray based techniques: XRD and XANES, respectively. The Rietveld refinement permitted to confirm the smectite phase and identify the complementary minerals of the commodity: quartz, gypsum and feldspars. The refinement allowed to quantify these phases and confirmed the high smectite (Montmorillonite type) content (≈90%).

A thermal analysis (DTA-TG-DTG) was employed for determining the bentonite thermal transformations ant to ensure the dehydration and dehydroxylation of the clay mineral. Results were consistent with the XRD-Rietveld and the chemical composition.

Both aluminum and silicon atoms in the different materials were locally described and compared by Al/Si XANES. Both coordination geometries and first neighbor environment were established in each material and consistently compared with further studies on aluminum and silicon materials and minerals. On the other hand, the smectitic interlayer thermal displacement was also evaluated (from 9.81 to 15.49 Å) by XRD. The silicon tetra coordination was confirmed in both materials; the aluminum tetra and hexa-coordination was found in both materials. The expected higher Al^{IV}/Al^{VI} ratio was confirmed and pondered for the thermally treated bentonite.

The features of the evaluated (Al/Si K-XANES) spectra could be employed for characterization and evaluation of more mild differences between similar materials and/or minerals like in chemical or physical modifications, usually performed for different technological applications, like in organo-clays, pillared clays, catalysts, and adsorbents.

Acknowledgments

The authors are grateful to the support of LNLS (SXS-18023). L.A. and F.G.R acknowledge the support of PIP-1035. N.M.R acknowledges the support of PICT-0778 and PICT-0672.

References

Abu-Zreig, M.M., Al-Akhras, N.M., Attom, M.F., 2001. Influence of heat treatment on the behavior of clayey soils. Appl. Clay Sci. 20:129–135. http://dx.doi.org/10.1016/S0169-1317(01)00066-7.

Andrini, L., Angelomé, P.C., Soler-Illia, G.J.A.A., Requejo, F.G., 2016a. Understanding the Zr and Si interdispersion in Zr1– xSixO2 mesoporous thin films by using FTIR and XANES spectroscopy. Dalton Trans. 45:9977–9987. http://dx.doi.org/10.1039/C6DT00203J.

Andrini, L., Gauna, M.R., Conconi, M.S., Suarez, G., Requejo, F.G., Aglietti, E.F., Rendtorff, N.M., 2016b. Extended and local structural description of a kaolinitic clay, its fired ceramics and intermediates: an XRD and XANES analysis. Appl. Clay Sci. 124–125: 39–45. http://dx.doi.org/10.1016/j.clay.2016.01.049.

Barrer, R.M., 1989. Shape-selective sorbents based on clay minerals: a review1. Clay Clay Miner. 37:385–395. http://dx.doi.org/10.1346/CCMN.1989.0370501.

Besq, A., Malfoy, C., Pantet, A., Monnet, P., Righi, D., 2003. Physicochemical characterisation and flow properties of some bentonite muds. Appl. Clay Sci. 23:275–286. http://dx.doi.org/10.1016/S0169-1317(03)00127-3.

Christidis, G.E., 1998. Physical and chemical properties of some bentonite deposits of Kimolos Island, Greece. Appl. Clay Sci. 13:79–98. http://dx.doi.org/10.1016/S0169-1317(98)00023-4.

Conconi, M.S., Gauna, M.R., Serra, M.F., Suarez, G., Aglietti, E.F., Rendtorff, N.M., 2014. Quantitative firing transformations of a triaxial ceramic by X-ray diffraction methods. Cerâmica 60:524–531. http://dx.doi.org/10.1590/S0366-69132014000400010.

Divakar, D., Manikandan, D., Kalidoss, G., Sivakumar, T., 2008. Hydrogenation of benzaldehyde over palladium intercalated bentonite catalysts: kinetic studies. Catal. Lett. 125: 277. http://dx.doi.org/10.1007/s10562-008-9532-3.

Drits, V.A., Besson, G., Muller, F., 1995. An improved model for structural transformations of heat-treated aluminous dioctahedral 2:1 layer silicates. Clay Clay Miner. 43, 718–731.

Fendorf, S.E., Sparks, D.L., Lamble, G.M., Kelley, M.J., 1994. Applications of X-ray absorption fine structure spectroscopy to soils. Soil Sci. Soc. Am. J. 58:1583. http://dx.doi.org/10.2136/sssaj1994.03615995005800060001x.

Garvie, L.A.J., Buseck, P.R., 1999. Bonding in silicates; investigation of the Si L (sub 2,3) edge by parallel electron energy-loss spectroscopy. Am. Mineral. 84:946–964. http://dx.doi.org/10.2138/am-1999-5-631.

Grim, R.E., Güven, N., 1978. Bentonites geology, mineralogy, properties and uses. Elsevier Scientific Pub. Co.; Distributors for the United States and Canada, Elsevier/North-Holland, Amsterdam; New York; New York.

Gunay, E., Ozkan, T.O., 2001. Production of porous ramics from sepiolite based minerals. Ind. Ceram. 21, 145–149.

Henderson, G.S., de Groot, F.M.F., Moulton, B.J.A., 2014. X-ray absorption near-edge structure (XANES) spectroscopy. Rev. Mineral. Geochem. 78:75–138. http://dx.doi.org/10.2138/rmg.2014.78.3.

Ildefonse, P., Cabaret, D., Sainctavit, P., Calas, G., Flank, A.-M., Lagarde, P., 1998. Aluminium X-ray absorption near edge structure in model compounds and Earth's surface minerals. Phys. Chem. Miner. 25:112–121. http://dx.doi.org/10.1007/s002690050093.

Kato, Y., Shimizu, K., Matsushita, N., Yoshida, T., Yoshida, H., Satsuma, A., Hattori, T., 2001. Quantification of aluminium coordinations in alumina and silica–alumina by Al K-edge XANES. Phys. Chem. Chem. Phys. 3:1925–1929. http://dx.doi.org/10.1039/b100610j.

Komadel, P., 2016. Chemically modified smectites. Clay Miner. 38:127–138. http://dx.doi.org/10.1180/0009855033810083.

Li, D., Bancroft, G.M., Fleet, M.E., 1996. Coordination of Si in Na 2 O–SiO 2–P 2 O 5 glasses using Si K- and L-edge XANES. Am. Mineral. 81:111–118. http://dx.doi.org/10.2138/am-1996-1-214.

Li, D., Bancroft, G.M., Fleet, M.E., Feng, X.H., Pan, Y., 1995. Al K-edge XANES spectra of aluminosilicate minerals. Am. Mineral. 80:432–440. http://dx.doi.org/10.2138/am-1995-5-602.

Li, D., Bancroft, G.M., Kasrai, M., Fleet, M.E., Feng, X.H., Tan, K.H., Yang, B.X., 1993. High-resolution Si K- and L2,3-edge XANES of α-quartz and stishovite. Solid State Commun. 87:613–617. http://dx.doi.org/10.1016/0038-1098(93)90123-5.

Li, D., Bancroft, G.M., Kasrai, M., Fleet, M.E., Secco, R.A., Feng, X.H., Tan, K.H., Yang, B.X., 1994. X-ray absorption spectroscopy of silicon dioxide (SiO2) polymorphs; the structural characterization of opal. Am. Mineral. 79, 622–632.

Liu, P., 2007. Polymer modified clay minerals: a review. Appl. Clay Sci. 38:64–76. http://dx.doi.org/10.1016/j.clay.2007.01.004.

Mahmoud, S., 1999. Effect of acid activation on the de-tert-butylation activity of some Jordanian clays. Clay Clay Miner. 47:481–486. http://dx.doi.org/10.1346/CCMN.1999.0470410.

Murray, H.H., 2000. Traditional and new applications for kaolin, smectite, and palygorskite: a general overview. Appl. Clay Sci. 17:207–221. http://dx.doi.org/10.1016/S0169-1317(00)00016-8.

Önal, M., Sarıkaya, Y., 2007. Thermal behavior of a bentonite. J. Therm. Anal. Calorim. 90: 167–172. http://dx.doi.org/10.1007/s10973-005-7799-9.

Outka, D.A., Stöhr, J., 1988. Curve fitting analysis of near-edge core excitation spectra of free, adsorbed, and polymeric molecules. J. Chem. Phys. 88:3539–3554. http://dx.doi.org/10.1063/1.453902.

Pinnavaia, T.J., 1983. Intercalated clay catalysts. Science 220:365–371. http://dx.doi.org/10.1126/science.220.4595.365.

Ravel, B., Newville, M., 2005. *ATHENA*, *ARTEMIS*, *HEPHAESTUS*: data analysis for X-ray absorption spectroscopy using *IFEFFIT*. J. Synchrotron Radiat. 12:537–541. http://dx.doi.org/10.1107/S0909049505012719.

Reichle, W.T., 1985. Catalytic reactions by thermally activated, synthetic, anionic clay minerals. J. Catal. 94:547–557. http://dx.doi.org/10.1016/0021-9517(85)90219-2.

Reis, A.S., Ardisson, J.D., 2003. Exchangeable ion and thermal treatment effects on basal spacings of al-hydroxy pillared montmorillonites. Clay Clay Miner. 51:33–40. http://dx.doi.org/10.1346/CCMN.2003.510104.

Ressler, T., 1998. WinXAS: a program for X-ray absorption spectroscopy data analysis under MS-windows. J. Synchrotron Radiat. 5:118–122. http://dx.doi.org/10.1107/S0909049597019298.

Rietveld, H.M., 1969. A profile refinement method for nuclear and magnetic structures. J. Appl. Crystallogr. 2:65–71. http://dx.doi.org/10.1107/S0021889869006558.

Rodríguez-Carvajal, J., 2001. Recent developments of the program FULLPROF. Comm. Powder Diffr. IUCr Newsletter 26, pp. 12–19.

Romano, C., Paris, E., Poe, B.T., Giuli, G., Dingwell, D.B., Mottana, A., 2000. Effect of aluminum on Ti-coordination in silicate glasses: a XANES study. Am. Mineral. 85:108–117. http://dx.doi.org/10.2138/am-2000-0112.

Sarı Yılmaz, M., Kalpaklı, Y., Pişkin, S., 2013. Thermal behavior and dehydroxylation kinetics of naturally occurring sepiolite and bentonite. J. Therm. Anal. Calorim. 114: 1191–1199. http://dx.doi.org/10.1007/s10973-013-3152-x.

Sarikaya, Y., Önal, M., Baran, B., Alemdaroğlu, T., 2000. The effect of thermal treatment on some of the physicochemical properties of a bentonite. clay clay miner. 48, 557–562.

Serra, M.F., Conconi, M.S., Suarez, G., Agietti, E.F., Rendtorff, N.M., 2013. Firing transformations of an Argentinean calcareous commercial clay. Cerâmica 59:254–261. http://dx.doi.org/10.1590/S0366-69132013000200010.

Shaw, S.A., Peak, D., Hendry, M.J., 2009. Investigation of acidic dissolution of mixed clays between pH 1.0 and -3.0 using Si and Al X-ray absorption near edge structure. Geochim. Cosmochim. Acta 73:4151–4165. http://dx.doi.org/10.1016/j.gca.2009.04.004.

Tan, Ö., Yılmaz, L., Zaimoğlu, A.S., 2004. Variation of some engineering properties of clays with heat treatment. Mater. Lett. 58:1176–1179. http://dx.doi.org/10.1016/j.matlet.2003.08.030.

Vallés, J.M., Impiccini, A., 1999. Bentonitas de la Cuenca Neuquina, Río Negro, Neuquén y La Pampa. In: Zappettini, O. (Ed.), Recursos Minerales de la República Argentina. Instituto de Geología y Recursos Minerales. SEGEMAR, Anales 35, pp. 1113–1125.

Volzone, C., Sanchez, R.M.T., 1993. Thermal and mechanical effects on natural and activated smectite structure. Colloids Surf. A Physicochem. Eng. Asp. 81:211–216. http://dx.doi.org/10.1016/0927-7757(93)80248-D.

Wang, M., Benway, J., Arayssi, A., 1990. The effect of heating on engineering properties of clays. In: Hoddinott, K., Lamb, R. (Eds.), Physico-Chemical Aspects of Soil and Related Materials. ASTM International, 100 Barr Harbor Drive, PO Box C700, West Conshohocken, PA 19428–2959 (pp. 139–139–20_.

Zivica, V., Palou, M.T., 2015. Physico-chemical characterization of thermally treated bentonite. Compos. Part B 68:436–445. http://dx.doi.org/10.1016/j.compositesb.2014.07.019.